JOURNAL OF THERMOPHYSICS AND HEAT TRANSFER
Vol. 20, No. 1, January–March 2006

Model-Based Method of Theoretical Design Analysis of a Loop Heat Pipe

Masao Furukawa*
Japan Aerospace Exploration Agency, Tsukuba 305-8505, Japan

Mathematical models accepted so far for loop heat pipes (LHPs) are mentioned, with a brief account of the operating characteristics. The necessity of an analytical model formed in a consistent way is stressed from the viewpoint of design practices. An ordinary differential equation, expressing the heat and mass transfer in a thick-walled porous cylinder, is solved to give a radial temperature distribution of the cylindrical wick, from which the outside-to-inside wick diameter ratio is derived. This ratio depends on the number of transfer units and is finally expressed in terms of the evaporator temperature effectiveness, which serves as a performance index. Positive-powered expressions, including the specified critical Bond number and specified linear pressure loss gradients, are then given to determine the wick inside, vapor line, and liquid line diameters. A pressure-loss model, consisting of theoretically or empirically obtained practical expressions, is presented to specify the wick pore radius. Derived expressions for the wick permeability and conductivity are combined to find an optimal wick porosity. The degree of subcooling, determined from the heat leak and the heat loss or gain, is given in a binominal expression dependent on the heat load, operating temperature, ambient temperature, and modeled coupling conductances. That degree is then converted into the pump efficiency, serving as another performance index. A reasonable method for reservoir sizing is proposed, considering both hot and cold startups. A two-region model representing the surface activity of a condensing radiator is introduced to determine the condenser/subcooler tube diameter, the total tube length, and the radiator half feeder spacing. All the expressions are arranged to develop into an LHP design code of convenience. Results of numerical computations done over a possibly wide range of parameters are graphically shown in the figures with a view to offering LHP design curves of interest.

Nomenclature

A	=	area, m^2
Bo	=	Bond number
c	=	constant
c_p	=	specific heat at constant pressure, $J/kg \cdot K$
D	=	diameter, m
F	=	two-phase heat transfer coefficient multiplier
Fr	=	Froude number
f	=	factor
g	=	gravitational acceleration, 9.80665 m/s^2
h	=	heat transfer coefficient, $W/m^2 \cdot K$
K	=	thermal conductance, W/K
K_p	=	permeability, m^2
k	=	thermal conductivity, $W/m \cdot K$
L	=	length, m
M	=	mass, kg
Ma	=	Mach number
m	=	specific mass, kg/m
$\dot{m}$	=	mass flow rate, kg/s
NTU	=	number of transfer units
n	=	exponent
$\bar{n}$	=	reciprocal of NTU
p	=	pressure, Pa
Q	=	heat load, W
Q'	=	heat gain, W
q	=	heat load density, W/m^2
r	=	radius or radial distance, m
$\mathcal{R}$	=	diameter ratio
S_u	=	ultimate tensile stress, Pa
T	=	temperature, K
U	=	overall heat transfer coefficient, $W/m^2 \cdot K$
V	=	volume, m^3
v	=	velocity, m/s
W	=	width or spacing, m
We	=	Weber number
z	=	magnified density ratio
α	=	volume ratio or void fraction
β	=	volume ratio or conductivity ratio
Γ	=	region length ratio
γ	=	latent to sensible heat ratio or specific heat ratio
δ	=	thickness, m
ε	=	porosity, emittance, diameter ratio, or area ratio
ζ	=	pressure loss coefficient
η	=	efficiency, effectiveness, or normalized region length
λ	=	latent heat of vaporization, J/kg
μ	=	dynamic viscosity, $Pa \cdot s$
ν	=	kinematic viscosity, m^2/s
ρ	=	mass density, kg/m^3
σ	=	surface tension, N/m
$\bar{\sigma}$	=	Stefan-Boltzmann constant, $5.6687 \cdot 10^{-8}$ $W/m^2 \cdot K^4$
Φ	=	temperature effectiveness
ϕ^2	=	two-phase friction factor multiplier
φ	=	cross-sectional area ratio
χ	=	vapor quality (dryness fraction)
ψ	=	averaged friction factor multiplier
ω	=	conduction parameter

Subscripts

Al	=	aluminum
a	=	ambient
ann	=	annular space
bayo	=	bayonet tube
c	=	capillary pore
cap	=	capillary
cont	=	contraction
cond	=	condenser

Received 18 November 2004; revision received 13 April 2005; accepted for publication 30 April 2005.

*Invited Researcher, ETS-VIII Project Team, Tsukuba Space Center, 2-1-1, Sengen; also working for Japan Manned Space Systems Corporaton. Senior Member AIAA.

dry = dry (not including coolant)
eff = effective
evap = evaporator
F = fin
FL = fluid line
fitt = fittings
grav = gravitational
H = pump head
h = heat transfer surface
in = inside
inv = inventory
L = liquid
LL = liquid line
l = saturated liquid
lch = liquid channel
lm = logarithmic mean
loop = fluid loop
out = outside
P = pump or plate
port = vapor exit port
R = radiation or radiator
r = radial
rad = radiator panel
res = reservoir (compensation chamber)
S = heat sink or radiative surface
sub = subcooling or subcooler
t = thermal infrared
V = vapor
VL = vapor line
v = saturated vapor
vch = vapor channel (grooves)
w = wick
wet = wet (including coolant)
wick = capillary wick
1ϕ = single-phase (subcooled)
2ϕ = two-phase (condensing)
$\perp$ = radially evaluated or thicknesswise

Superscripts

$*$ = critical or design-specified
- = averaged or reference
, = differentiated or modified
(a) = active zone
(l) = liquid
(v) = vapor

Introduction

AS spacecraft mission requirements become more complex and the equipment power density increasingly goes up, thermal design cases frequently occur where we are forced to replace traditional heat pipes with innovative heat-transfer devices. This is because heat pipes are essentially low in heat-transport capacity and permit no arrangements other than parallel or cross lines. Most promising among such innovative devices are CPLs (capillary pump loops)[1] and LHPs (loop heat pipes).[2,3] The CPL, proposed by Stenger,[4] has been developed in the United States and Europe, whereas the LHP, invented by Maidanik et al.[5] under the name of AGHP (antigravitational heat pipe), has gained acceptance mainly in Russia. Both are alike in operation principle and components layout. Each basically consists of a capillary pump evaporator with reservoir and a condensing radiator. They are connected to form a loop with small-diameter tubes bendable at will, thereby permitting us to set up the radiator at a specified position. Then, due to the employed microporous wicks, both CPLs and LHPs can transport heat over long distances and may produce a capillary pressure rise exceeding the gravitational head. As pointed out by Nikitkin and Cullimore,[6] a noticeable difference between CPLs and LHPs is the way of installing a two-phase reservoir. In most CPLs, the reservoir is remotely connected with the evaporator inlet through a plumb line and is usually heated before startup to assuredly maintain liquid in the wick. In contrast, the reservoir in LHPs, initially called compensation chamber[7] or hydroaccumulator,[2] may contain some wicks structurally connected with the evaporator liquid-core portion. This capillary connection gets the loop ready for start and thereby, unlike CPLs, LHPs need neither preconditioning nor starter pumps. Thus, LHPs are inherently passive and have advantages such as large permissible adverse tilts, compliance with complicated layouts, and zonal separation of heat acquisition and rejection. Such remarkable merits induced Maidanik et al.[7] and Wolf et al.[8] to survey the prospects and potentials of LHPs for space applications. As expected, the LHP technology has become popular and is rapidly being accepted in spacecraft thermal control. The LHPs flown with success are Alyona aboard Granat[9] in 1989, Obzor[10] in 1994, Mars 96[11] in 1996, LHPFX[12] aboard STS-87 in 1997, and ALPHA[13] aboard STS-83 and STS-94 in 1997. Also mentioned are LHPs for NASA's GLAS,[14] CNES's STENTOR,[15] ESA's COM2PLEX,[16] and high-power communications satellites. It is then added that miniature,[17] reversible,[18] and multiple evaporator[19,20] LHPs have recently appeared as evolved versions of classical ones.

Studies on operating characteristics of LHPs have naturally kept pace with various development works stated above. First, Maidanik et al.[5,7] expressed the LHP working cycle in a pressure versus temperature diagram and they[7] derived a thermohydraulic relation from there. That relation is also presented by Ku.[21] Wolf and Bienert[22] then investigated the temperature-control characteristics of LHPs and found that the LHP could work in variable-conductance mode at lower powers, whereas in fixed-conductance mode it worked at higher loads. A graphical relation between the temperature and the power thus becomes V-shaped, as mentioned by Sasin et al.[23] and Goncharov et al.[24] Most test results[21,25–27] give similar performance curves. This distinctive feature, called autoregulation,[22,25] results from conductive coupling between the reservoir and the evaporator; therefore, its rate can be a significant design parameter. LHPs are self-starting devices but there still exist some conditions for reliable startup. Baumann et al.[28,29] extensively examined the effects of gas, mass, and tilt on startups with analysis tools. Gluck et al.[30] showed that cold startups are not always successful. Ku et al.[31,32] experimentally studied low-power operations. Many attempts have been made on the LHP modeling to have a better understanding of test results. Bienert and Wolf[33] took a lumped-parameter approach in solving concurrent pressure and energy balances. Kaya and his coworkers[34,35] developed a mathematical model for steady-state analysis and experimentally validated it. Hoang and Kaya[36] improved a two-phase pressure-drop model for more precise predictions of the LHP operating temperature. To accurately simulate the characteristics, Wrenn et al.[37] prepared a transient LHP model and verified it by comparison of predicted and measured temperatures. For both steady-state and transient analyses, Cullimore and Baumann[38] developed a more detailed LHP model based on SINDA/FLUINT. Pauken and Rodriguez[39] applied that nodal network model to performance predictions of ammonia- or propylene-filled LHPs and experimentally demonstrated its validity. Further demonstration was done by Hoff and Rogers[40] in SINDA/FLUINT model correlation. Such computational models[38–40] are thus acceptable for LHP thermohydraulic state predictions.

Now, as easily seen, there can be two kinds of LHP models responding to the practically different purposes. All the models stated above[33–40] are of the first kind, in which the operating temperature is not given in advance but uniquely determined. Models of the second kind are such that the operating temperature is design-specified. This shows that the first generally serves simulation purposes, whereas the second is fitted for design or sizing problems. The latter should therefore be analytical rather than computational in form. Analytically expressed LHP models are found in early research works[23,41,42] but originally aimed at off-design state predictions, as done by the author.[43] Although heat and mass transfer analysis by Parker et al.[44] and Hoang and Ku[45] are helpful in preparing analytical models, almost no LHP models of our concern are available for the present. This probably comes from the circumstance that design practices mainly depend on manufacturers and the details of their methods are usually not open to the public. It is finally expected that some

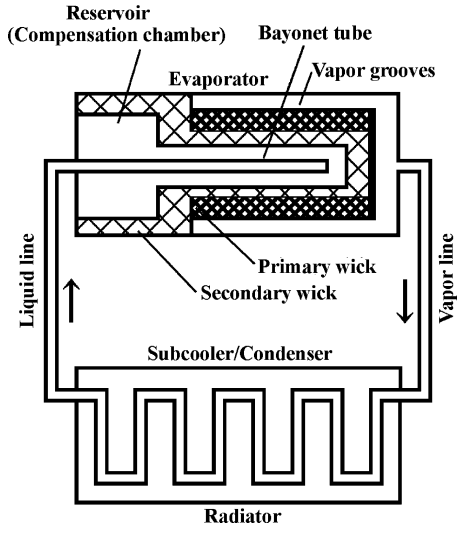

Fig. 1 Schematic of a loop heat pipe.

efforts would again be made of LHP design studies. To come up to such expectations, this study has been made with two objects. The first is to offer all the expressions necessary in LHP analytical modeling, most of which are newly obtained. The second is to provide engineers and researchers with a straightforward method of LHP design analysis.

Analytical Modeling

Figure 1 schematically shows a typical LHP consisting of an evaporator, a condenser/subcooler/radiator, a compensation chamber, hereafter called reservoir, and vapor and liquid transport lines. As shown in the figure, the evaporator and the reservoir are made in a body and contain wicks. Primary wick is laid to produce a capillary pump head, whereas secondary wick makes a liquid link between the evaporator and the reservoir. Wick pore sizes are thereby fine in the primary but larger in the secondary. The reservoir always holds two-phase fluid and controls the loop operating temperature. The primary wick is usually cylindrically shaped to include a liquid core, into which a bayonet tube is inserted, passing through the reservoir. A liquid annulus is thus formed in the evaporator. The outside primary wick surface, mated with the inside casing surface, is axially trimmed to become vapor grooves. The condenser/subcooler and transport lines are then made of smooth-wall tubing. In most cases, a flat-plate saddle is placed on the evaporator for thermally uniform loading. As heat is applied to the saddle, vaporization occurs in the evaporator, reducing the wick meniscus radius. Capillary forces are developed there to fill up liquid. Generated vapor leaves grooves and goes down to the condenser, where condensation and subcooling are taken place to reject heat by the radiator. Subcooled liquid then goes back to the evaporator. The LHP working cycle is thus completed by a normal circulation of fluid.

Since the LHP primary wick is usually a relatively long thick-walled cylinder, fluid and heat flow through there may be radially one-dimensional. An energy equation for the problem therefore becomes such as shown in the literature[23,44]:

$$c_{pl}\rho_l\left(v_r\frac{\mathrm{d}T}{\mathrm{d}r}\right)=k_{\mathrm{eff}}\left[\frac{1}{r}\frac{\mathrm{d}}{\mathrm{d}r}\left(r\frac{\mathrm{d}T}{\mathrm{d}r}\right)\right] \tag{1}$$

where r is the radial distance taken from the cylinder centerline, T the wick local temperature, v_r the fluid radial velocity, c_{pl} the liquid specific heat, ρ_l the liquid density, and k_{eff} the wick effective conductivity. Considering the fluid flow passing over a cylindrical surface situated at r, one finds the mass flow rate

$$\dot{m}=2\pi r L_{\mathrm{evap}}^{(a)}\rho_l v_r \tag{2}$$

where $L_{\mathrm{evap}}^{(a)}$ is the evaporator active zone length. Equation (1) is thereby reduced to

$$\frac{\mathrm{d}}{\mathrm{d}r}\left(r\frac{\mathrm{d}T}{\mathrm{d}r}\right)=\bar{n}\frac{\mathrm{d}T}{\mathrm{d}r} \tag{3}$$

where $\bar{n}$ is constant and expressed in

$$\bar{n}=\dot{m}c_{\mathrm{pl}}\big/2\pi L_{\mathrm{evap}}^{(a)}k_{\mathrm{eff}} \tag{4}$$

An analytical solution of Eq. (3), satisfying such boundary conditions as $T(r_{w\,\mathrm{in}})=T_{w\,\mathrm{in}}$ and $T(r_{w\,\mathrm{out}})=T_{w\,\mathrm{out}}$, is

$$(T-T_{w\,\mathrm{in}})/(T_{w\,\mathrm{out}}-T_{w\,\mathrm{in}})=\left(r^{\bar{n}}-r_{w\,\mathrm{in}}^{\bar{n}}\right)\Big/\left(r_{w\,\mathrm{out}}^{\bar{n}}-r_{w\,\mathrm{in}}^{\bar{n}}\right) \tag{5}$$

Solutions identical to Eq. (5) are given by Maidanik et al.[41] and Parker et al.[44] The heat transfer across the wick, from $r_{w\,\mathrm{out}}$ to $r_{w\,\mathrm{in}}$, can be determined from

$$K_{\mathrm{evap}}(T_{w\,\mathrm{out}}-T_{w\,\mathrm{in}})=k_{\mathrm{eff}}2\pi r_{w\,\mathrm{in}}L_{\mathrm{evap}}^{(a)}T'(r_{w\,\mathrm{in}}) \tag{6}$$

where K_{evap} is the evaporator radial conductance and $T'(r_{w\,\mathrm{in}})$ the temperature gradient at the wick inner surface. Due to Eq. (5), Eq. (6) turns into

$$K_{\mathrm{evap}}=\dot{m}c_{\mathrm{pl}}\big/\left(\mathcal{R}_w^{\bar{n}}-1\right) \tag{7}$$

where $\mathcal{R}_w$ is the wick outside-to-inside-diameter ratio,

$$\mathcal{R}_w=r_{w\,\mathrm{out}}/r_{w\,\mathrm{in}}=D_{w\,\mathrm{out}}/D_{w\,\mathrm{in}} \tag{8}$$

Basically the same expressions as Eq. (7) are found in the literature.[44,46]

Here, a concept of the number of transfer units is still available for performance evaluation because the LHP evaporator can be regarded as a heat exchanger. That number is generally defined in

$$\mathrm{NTU}_{\mathrm{evap}}=K_{\mathrm{evap}}/\dot{m}c_{\mathrm{pl}} \tag{9}$$

Substituting Eq. (7) into Eq. (9) gives

$$\mathrm{NTU}_{\mathrm{evap}}=1\big/\left(\mathcal{R}_w^{\bar{n}}-1\right) \tag{10}$$

Also derived from Eq. (6) is a practical expression for that conductance

$$K_{\mathrm{evap}}=2\pi L_{\mathrm{evap}}^{(a)}k_{\mathrm{eff}} \tag{11}$$

Applying Eq. (4) to the product of Eqs. (9) and (11) makes

$$\bar{n}\mathrm{NTU}_{\mathrm{evap}}=1 \tag{12}$$

Owing to this relation, Eq. (10) simply becomes

$$\mathcal{R}_w^{\bar{n}}=1+\bar{n} \tag{13}$$

The diameter ratio is therefore determined from

$$\mathcal{R}_w=\exp[\mathrm{NTU}_{\mathrm{evap}}\,\ell n(1+1/\mathrm{NTU}_{\mathrm{evap}})] \tag{14}$$

A performance index more convenient than $\mathrm{NTU}_{\mathrm{evap}}$ is the evaporator temperature effectiveness, Φ_{evap}. A well-known formula relating the two is

$$\Phi_{\mathrm{evap}}=1-\exp(-\mathrm{NTU}_{\mathrm{evap}}) \tag{15}$$

This expression readily leads to

$$\mathrm{NTU}_{\mathrm{evap}}=-\ell n(1-\Phi_{\mathrm{evap}}) \tag{16}$$

Because of the double-pipe construction of the LHP evaporator, the wick inside diameter $D_{w\,\mathrm{in}}$ is expressed as

$$D_{w\,\mathrm{in}}=D_{\mathrm{bayo}}+W_{\mathrm{ann}} \tag{17}$$

The bayonet tube diameter is then

$$D_{\text{bayo}} = D_{\text{LL}} \tag{18a}$$

where D_{LL} is the liquid line diameter. The Bond number of concern depends on the annular spacing W_{ann} formed between the cylindrical wick and the inserted tube. A defining expression for that number turns into

$$W_{\text{ann}} = \left[Bo^* \sigma_l \Big/ (\rho_l - \rho_v) g\right]^{\frac{1}{2}} \tag{18b}$$

where Bo^* is the critical Bond number for stable condensation, σ_l the liquid surface tension, ρ_v the vapor density, and g the gravitational acceleration. Such a value as $Bo^* \leq 12$ is derived from a relation, $Bo = We/Fr$, and critical Weber and Froude numbers, $We^* \leq 3$ and $Fr^* \geq 0.25$, found in the literature.[47,48] The wick outside diameter $D_{w\,\text{out}}$ and the wick thickness δ_w are determined from

$$D_{w\,\text{out}} = \mathcal{R}_w D_{w\,\text{in}} \tag{19a}$$

$$\delta_w = (\mathcal{R}_w - 1) D_{w\,\text{in}}/2 \tag{19b}$$

In proportion to the heat load Q, the evaporator length L_{evap} is sized as

$$L_{\text{evap}} = Q/(Q/L)^*_{\text{evap}} \tag{20}$$

For a saddled evaporator, the sizing parameter $(Q/L)^*_{\text{evap}}$ is given by

$$(Q/L)^*_{\text{evap}} = \left(L^{(a)} \Big/ L\right)^*_{\text{evap}} (W/D)^*_{\text{evap}} D_{w\,\text{out}} q \tag{21}$$

where $(L^{(a)}/L)^*_{\text{evap}}$ is the active zone–to–total length ratio, $(W/D)^*_{\text{evap}}$ the saddle width–to–evaporator diameter ratio, and q the heat-load density. Dimensions of the LHP evaporator can thus be uniquely specified for a separately determined D_{LL} value.

A loop pressure-loss estimate is now made to find a required capillary pump head. The loop pressure loss Δp_{loop}, originated in a layout shown in Fig. 1, is expressed in

$$\Delta p_{\text{loop}} = \Delta p_{\text{VL}} + \Delta p_{\text{LL}} + \Delta p_{\text{cond}} + \Delta p^{(l)}_{\text{evap}} + \Delta p^{(v)}_{\text{evap}} + \Delta p_{\text{port}} + \Delta p_{\text{fitt}} \tag{22}$$

where Δp_{VL} is the vapor-line loss, Δp_{LL} the liquid-line loss, Δp_{cond} the condenser-tube loss, $\Delta p^{(l)}_{\text{evap}}$ the evaporator liquid-channel loss, $\Delta p^{(v)}_{\text{evap}}$ the evaporator vapor-grooves loss, Δp_{port} the evaporator exit-port loss, and Δp_{fitt} the evaporator/condenser-fitting loss. The line and condenser losses are then estimated as

$$\Delta p_{\text{VL}} = (\Delta p_{\text{VL}}/L_{\text{VL}})^* L_{\text{VL}} \tag{23a}$$

$$\Delta p_{\text{LL}} = (\Delta p_{\text{LL}}/L_{\text{LL}})^* L_{\text{LL}} \tag{23b}$$

$$\Delta p_{\text{cond}} = (\Delta p_{\text{cond}}/Q)^* (Q + Q') \tag{23c}$$

where L_{VL} is the vapor-line length, L_{LL} the liquid-line length, and Q' the heat gain through the reservoir. In calculating Eqs. (23a–23c), empirically accepted possible values will first be assigned to the line pressure-loss gradients, $(\Delta p_{\text{VL}}/L_{\text{VL}})^*$ and $(\Delta p_{\text{LL}}/L_{\text{LL}})^*$, and the condenser pressure-loss rate, $(\Delta p_{\text{cond}}/Q)^*$. The last four terms of Eq. (22) are analytically expressed in

$$\Delta p_{\text{evap}} = \Delta p^{(l)}_{\text{evap}} + \Delta p^{(v)}_{\text{evap}}$$

$$= \zeta_{\text{evap}} \left(64/\pi D^4_{\text{bayo}}\right) (\nu_l/\lambda) \left[Q^2/(Q/L)^*_{\text{evap}}\right] \tag{24a}$$

$$\Delta p_{\text{port}} = \zeta_{\text{port}} Ma^{*2} \gamma_v p_v \Big/ 2 \tag{24b}$$

$$\Delta p_{\text{fitt}} = \left(\zeta^{(v)}_{\text{fitt}} \Big/ \rho_v D^4_{\text{VL}} + \zeta^{(l)}_{\text{fitt}} \varphi^2_{\text{cond/LL}} \Big/ \rho_l D^4_{\text{LL}}\right) (8/\pi^2)(Q/\lambda)^2 \tag{24c}$$

where ν_l is the liquid kinematic viscosity, λ the latent heat of vaporization, γ_v the vapor specific-heat ratio, and p_v the vapor pressure. Derived practical expressions for the pressure-loss coefficients, ζ_{evap}, ζ_{port}, $\zeta^{(v)}_{\text{fitt}}$, and $\zeta^{(l)}_{\text{fitt}}$, are respectively given in Eqs. (A1a), (A2a), (A3a), and (A4a) of Appendix A, the latter three of which are commonly expressed as Eq. (A5a). In deriving those coefficients, one introduces Eqs. (A1b), (A2b), (A3b), and (A4b) to define the related cross-sectional area ratios. The factor $\varphi_{\text{cond/LL}}$ in Eq. (24c), defined in Eq. (A4b), shows a change of section at the condenser exit. Equation (24b), including a squared Mach number, results from the relation that the pressure loss is proportional to a square of the vapor velocity. Because that speed is usually very low, we have specified Ma^* to be $1/1000\varepsilon_{\text{vch}}$, where the factor ε_{vch} is defined in Eq. (A2c). Considering the wick loss Δp_{wick} and the gravitational loss Δp_{grav}, the required capillary pump head Δp_{cap} is given by

$$\Delta p_{\text{cap}} = f_H \Delta p_{\text{loop}} + \Delta p_{\text{wick}} + \Delta p_{\text{grav}} \tag{25}$$

where f_H is the head factor showing a pump capacity margin. If menisci formed on the outside wick surface fully draw back into the capillary pores under a pressure balance expressed in Eq. (25), the pump head then becomes

$$\Delta p_{\text{cap}} = 2\sigma_l/r_c \tag{26}$$

where r_c is the capillary pore radius. Introducing the wick loss–to–pump head ratio $(\Delta p_{\text{wick}}/\Delta p_{\text{cap}})^*$, one has

$$\Delta p_{\text{wick}} = (\Delta p_{\text{wick}}/\Delta p_{\text{cap}})^* \Delta p_{\text{cap}} \tag{27}$$

Substituting Eqs. (26) and (27) into Eq. (25) gives

$$r_c = 2\sigma_l \left[1 - (\Delta p_{\text{wick}}/\Delta p_{\text{cap}})^*\right] \Big/ (f_H \Delta p_{\text{loop}} + \Delta p_{\text{grav}}) \tag{28}$$

A required wick pore radius can thus be found.

Applying the Darcy's law to the wick-permeating liquid flow and considering again Eq. (2), one obtains a radial pressure gradient $\mathrm{d}p/\mathrm{d}r$. Integrating it over the range from $r_{w\,\text{in}}$ to $r_{w\,\text{out}}$ results in

$$\Delta p_{\text{wick}} = \nu_l \dot{m} \Big/ 2\pi L^{(a)}_{\text{evap}} K_{p\perp} \tag{29}$$

where $K_{p\perp}$ differs from the wick characteristic permeability K_p and is defined in

$$K_{p\perp} = K_p / \ell_n \mathcal{R}_w \tag{30}$$

Equations (27) and (29) are combined to give

$$K_{p\perp} = \nu_l \dot{m} \Big/ 2\pi L^{(a)}_{\text{evap}} (\Delta p_{\text{wick}}/\Delta p_{\text{cap}})^* \Delta p_{\text{cap}} \tag{31}$$

Empirical expressions for K_p are various, as shown in the literature,[49,50] but most of them are of the Blake–Kozeny form,

$$K_p = r_c^2 \varepsilon_w^3 \Big/ c_w (1 - \varepsilon_w)^n \tag{32}$$

where ε_w is the wick porosity, n the exponent, and c_w the constant. Recommendable values cited from the literature are 1) $n = 2$ and $c_w = 30.5$ for fiber,[49–51] 2) $n = 2$ and $c_w = 37.5$ for powder,[49,50,52,53] and 3) $n = 2$ and $c_w = 43.2$ for beads.[54] Such values as $n = 0$ and $c_w = 54$ for foam are regressively obtained from Yip's data.[55] A relation between K_p and k_{eff} will be found in the following way. Substituting Eq. (11) into Eq. (9) yields

$$k_{\text{eff}} = \text{NTU}_{\text{evap}} \dot{m} c_{\text{pl}} \Big/ 2\pi L^{(a)}_{\text{evap}} \tag{33}$$

Dividing Eq. (33) by Eq. (31) yields

$$k_{\text{eff}}/K_{p\perp} = \text{NTU}_{\text{evap}} (c_{\text{pl}}/\nu_l) (\Delta p_{\text{wick}}/\Delta p_{\text{cap}})^* \Delta p_{\text{cap}} \tag{34}$$

Equation (30) is then intentionally rewritten as

$$k_{\text{eff}} \Big/ \left(K_p/r_c^2\right) = (k_{\text{eff}}/K_{p\perp}) r_c^2 \Big/ \ell_n \mathcal{R}_w \tag{35}$$

It should be noted that the right-hand side of Eq. (35) depends on Φ_{evap}, $(\Delta p_{\text{wick}}/\Delta p_{\text{cap}})^*$, and f_H and is calculated from Eqs. (14), (28), and (34). Empirical expressions of k_{eff}, found in the literatue,[49,50,56–58] are summarized in Appendix B. Employed are Eq. (B1a) for mesh/screen,[49,50,56] Eq. (B1b) for sintered fiber,[57]

Eq. (B2a) for powder,[50,56] Eq. (B2b) for sintered powder,[57] Eq. (B3) for beads,[49] and Eq. (B4) for foam.[58] A required wick porosity can thus be calculated from Eq. (35) with Eq. (32) and a most suitable expression in Appendix B.

Then, as seen from the pressure-versus-temperature diagram,[21] there exist three saturation states in an LHP. They are found in the condenser, the evaporator, and the reservoir, but attention is directed to states in the latter two. Taking notice of the liquid pressure p_l, one finds such relations as $p_{\text{evap}} = p_l + \Delta p_{\text{cap}}$ and $p_{\text{res}} = p_l + \Delta p_{\text{wick}}$ under the design condition. A pressure differential between the evaporator and the reservoir therefore becomes $\Delta p_{\text{cap}} - \Delta p_{\text{wick}}$. This causes a slight temperature difference in the secondary wick,

$$\Delta T_{\text{wick}} = (\Delta p_{\text{cap}} - \Delta p_{\text{wick}}) T_v'(p_v) \tag{36}$$

where $T_v'(p_v)$ is the p–T curve slope viewed from the pressure axis. Equation (36) is basically the same as given by Kaya et al.[34] and Kaya and Hoang[35] but, due to Eq. (25), the expression becomes

$$\Delta T_{\text{wick}} = (f_H \Delta p_{\text{loop}} + \Delta p_{\text{grav}}) / p_v'(T_v) \tag{37}$$

where $p_v'(T_v)$, a reciprocal of $T_v'(p_v)$, is the p–T curve slope evaluated at the vapor temperature T_v and can be calculated from the Clausius–Clapeyron equation. In steady states, most of the imposed heat Q can be removed from the evaporaror by phase change of the coolant, but part of it will be leaked out to the reservoir. One therefore obtains

$$Q = \dot{m}(\lambda + c_{\text{pl}} \Delta T_{\text{wick}}) \tag{38}$$

The heat inflow or outflow through the reservoir, examined by Ku,[21] Wrenn et al.,[37] and Hoang and Ku,[45] is also considered in a system energy balance. This heat gain or loss is approximately given by

$$Q' = K_{aw}(T_a - T_v) \tag{39}$$

where K_{aw} is the thermal conductance between the environment and the secondary wick and T_a the ambient temperature. Equation (39) becomes negative if $T_a < T_v$ but we put Q' zero in such cases. This comes from the design philosophy that condensers and radiators should be somewhat oversized. As discussed by Parker et al.,[44] the subcooling is still necessary because the heat gain Q' should be absorbed by the return liquid. That relation is expressed in

$$Q' = \dot{m} c_{\text{pl}} \Delta T_{\text{sub}} \tag{40}$$

where ΔT_{sub} is the degree of subcooling. Dividing Eq. (40) by Eq. (38) gives

$$\Delta T_{\text{sub}} = (Q'/Q)(\lambda / c_{\text{pl}} + \Delta T_{\text{wick}}) \tag{41}$$

The latent-to-sensible heat ratio then becomes

$$\gamma = \lambda / c_{\text{pl}} \Delta T_{\text{sub}} \tag{42}$$

When regarding the LHP as a thermal pump, one finds that the heat input amounts to $Q + Q'$ but used for pumping is $\dot{m}\lambda$. The pumping efficiency is thereby defined in

$$\eta_P = \dot{m}\lambda / (Q + Q') \tag{43}$$

Substituting Eqs. (38) and (40) into Eq. (43) results in

$$\eta_P = \gamma / (\gamma + 1 + \Delta T_{\text{wick}} / \Delta T_{\text{sub}}) \tag{44}$$

Supposing that the flow is turbulent in the vapor line but laminar in the liquid line and characterizing that by the Colburn friction factor expression, one obtains

$$\Delta p_{\text{VL}} = (1.12/\pi^{1.8}) \left(\mu_v^{0.2} \big/ \rho_v\right) \left(L_{\text{VL}} \big/ D_{\text{VL}}^{4.8}\right) \dot{m}^{1.8} \tag{45a}$$

$$\Delta p_{\text{LL}} = (128/\pi) \nu_l \left(L_{\text{LL}} \big/ D_{\text{LL}}^4\right) \dot{m} \tag{45b}$$

where μ_v is the vapor dynamic viscosity and D_{VL} the vapor line diameter. The mass flow rate $\dot{m}$ is simply derived from Eq. (38) to become

$$\dot{m} = Q / (\lambda + c_{\text{pl}} \Delta T_{\text{wick}}) \approx Q / \lambda \tag{46}$$

Applying Eq. (46) to Eqs. (45a) and (45b) yields

$$D_{\text{VL}} = \left[(1.12/\pi^{1.8}) \left(\mu_v^{0.2} \big/ \rho_v \lambda^{1.8}\right) Q^{1.8} \big/ (\Delta p_{\text{VL}} / L_{\text{VL}})^*\right]^{0.208} \tag{47a}$$

$$D_{\text{LL}} = 2\left[(8/\pi)(\nu_l/\lambda) Q \big/ (\Delta p_{\text{LL}} / L_{\text{LL}})^*\right]^{\frac{1}{4}} \tag{47b}$$

The bayonet tube diameter, specified in Eq. (18a), can thus be determined from Eq. (47b). Equations (47a) and (47b) are also used in condenser tube diameter and length sizing. To develop a practical way of sizing, one employs a two-region model consisting of a condensing vapor section and a subcooled liquid section. The normalized dimensionless lengths, $\eta_{2\phi}$ and $\eta_{1\phi}$, are then introduced to define an extent of the two-phase region and that of the single-phase region. The heat is rejected at the rate of $\dot{m}\lambda$ from the region of $\eta_{2\phi}$ but at the rate of $\dot{m} c_{\text{pl}} \Delta T_{\text{sub}}$ from the region of $\eta_{1\phi}$. Because the axial heat rejection can be equal to the radial heat transfer from the working fluid to the condenser tube, one finds

$$\dot{m}\lambda = \eta_{2\phi} A_h U_{2\phi} (\Delta T_\perp + \Delta T_{\text{sub}}) \tag{48a}$$

$$\dot{m} c_{\text{pl}} \Delta T_{\text{sub}} = \eta_{1\phi} A_h U_{1\phi} \Delta T_{\text{lm}} \tag{48b}$$

where A_h is the heat transfer surface area, $U_{2\phi}$ the overall heat transfer coefficient of the active condenser section, $U_{1\phi}$ that of the subcooler section, $\Delta T_\perp$ the exit liquid to radiator temperature difference, and ΔT_{lm} the logarithmic mean temperature difference. Those differences depend on ΔT_{sub} and are expressed in

$$\Delta T_\perp = \Delta T_{\text{sub}} / \Phi_{\text{sub}} \tag{49a}$$

$$\Delta T_{\text{lm}} = \Delta T_{\text{sub}} / \ell n(1 + \Phi_{\text{sub}}) \tag{49b}$$

where Φ_{sub} is the subcooler temperature effectiveness. Because $U_{2\phi}$ and $U_{1\phi}$ may respectively regarded as the film coefficients, $h_{2\phi}$ and $h_{1\phi}$, of the two- and single-phase heat transfer, the ratio $U_{2\phi}/U_{1\phi}$ is approximated as

$$U_{2\phi}/U_{1\phi} \approx h_{2\phi}/h_{1\phi} = \bar{F} \tag{50}$$

The averaged two-phase heat transfer coefficient multiplier $\bar{F}$ is calculated from Eq. (A7b) with Eq. (A6b). Dividing Eq. (48a) by Eq. (48b) gives the dimensionless length ratio. Due to Eqs. (49a), (49b), and (50), that ratio simply becomes

$$\Gamma = \eta_{2\phi}/\eta_{1\phi} = \gamma \Phi_{\text{sub}} / \bar{F}(1 + \Phi_{\text{sub}}) \ell n(1 + \Phi_{\text{sub}}) \tag{51}$$

It follows that

$$\eta_{2\phi} = \Gamma/(\Gamma + 1) \tag{52a}$$

$$\eta_{1\phi} = 1/(\Gamma + 1) \tag{52b}$$

A requirement that D_{VL} be larger than D_{LL} leads to the relation $D_{\text{VL}} > D_{\text{cond}} > D_{\text{LL}}$. The condenser tube diameter is therefore specified in

$$D_{\text{cond}} = \eta_{2\phi} D_{\text{VL}} + \eta_{1\phi} D_{\text{LL}} \tag{53}$$

The two-region model is also used to evaluate the active condenser loss and the subcooler loss. The sum of the two gives the total condenser loss,

$$\Delta p_{\text{cond}} = \psi \eta_{2\phi} \Delta p_{\text{cond}}^{(v)} + \eta_{1\phi} \Delta p_{\text{cond}}^{(l)} \tag{54a}$$

where ψ is the averaged two-phase friction factor multiplier and is calculated from Eq. (A8b). Since $\Delta p_{\text{cond}}^{(v)}$ and $\Delta p_{\text{cond}}^{(l)}$ are respectively

the same as Eqs. (45a) and (45b) in form and Eq. (46) holds, the vapor-to-liquid region loss ratio results in

$$\Delta p_{\text{cond}}^{(v)} \Big/ \Delta p_{\text{cond}}^{(l)} = (1.12/128\pi^{0.8})\left(\mu_v^{0.2} \Big/ \rho_v \nu_l \lambda^{0.8}\right) Q^{0.8} \Big/ D_{\text{cond}}^{0.8} \tag{54b}$$

Recalling that $(\Delta p_{\text{cond}}/Q)^*$ and $(\Delta p_{\text{LL}}/L_{\text{LL}})^*$ are design-specified and the required heat rejection amounts to $Q + Q'$, one has

$$\Delta p_{\text{cond}} \Big/ \Delta p_{\text{LL}} = \left[(\Delta p_{\text{cond}}/Q)^* \Big/ (\Delta p_{\text{LL}}/L_{\text{LL}})^*\right](Q + Q')/L_{\text{LL}} \tag{55a}$$

Considering Eq. (45b), the similarity between $\Delta p_{\text{cond}}^{(l)}$ and Δp_{LL} gives

$$\Delta p_{\text{cond}}^{(l)} \Big/ \Delta p_{\text{LL}} = (L_{\text{cond}}/L_{\text{LL}})/(D_{\text{cond}}/D_{\text{LL}})^4 \tag{55b}$$

As regards $\Delta p_{\text{cond}}/\Delta p_{\text{cond}}^{(l)}$, the expression is derived from Eq. (54a) and also from Eqs. (55a) and (55b). Equating those two yields the required total condenser length,

$$L_{\text{cond}} = \left[(\Delta p_{\text{cond}}/Q)^* \Big/ (\Delta p_{\text{LL}}/L_{\text{LL}})^*\right](D_{\text{cond}}/D_{\text{LL}})^4 \cdot (Q + Q') \Big/ \left(\psi \eta_{2\phi} \Delta p_{\text{cond}}^{(v)} \Big/ \Delta p_{\text{cond}}^{(l)} + \eta_{1\phi}\right) \tag{56}$$

One can thus calculate the condenser volume V_{cond} from Eqs. (53) and (56), the vapor-line volume V_{VL} from Eq. (47a), and the liquid-line volume V_{LL} from Eqs. (47b). The required reservoir volume V_{res} depends on the liquid swing volume, because the condenser and the vapor line are completely flooded under cold cases but never flooded under hot cases. Then, as mentioned by Ku[21] and Mishkinis et al.,[59] some liquid must remain in the reservoir at cold start, and some vapor must be left over there at hot start. Because the volumetric fluid inventory V_{inv} may practically be conserved, such requirements are written as

$$V_{\text{inv}} = V_{\text{evap}}^{(l)} + V_{\text{cond}} + V_{\text{VL}} + V_{\text{LL}} + \alpha_L V_{\text{res}} \qquad \text{at cold start} \tag{57a}$$

$$V_{\text{inv}} = V_{\text{evap}}^{(l)} + V_{\text{LL}} + (1 - \beta_V) V_{\text{res}} \qquad \text{at hot start} \tag{57b}$$

where $V_{\text{evap}}^{(l)}$ is the evaporator liquid channel volume, α_L the fill-up fraction of reservoir volume, and β_V the void fraction of it. Equations (57a) and (57b) are reduced to

$$V_{\text{res}} = (V_{\text{cond}} + V_{\text{VL}})/(1 - \alpha_L - \beta_V) \tag{58}$$

If $\alpha_L = \beta_V = 0.1$, Eqs. (57b) and (58) then become

$$V_{\text{inv}} = V_{\text{evap}}^{(l)} + V_{\text{LL}} + 0.9 V_{\text{res}} \tag{59a}$$

$$V_{\text{res}} = 1.25(V_{\text{cond}} + V_{\text{VL}}) \tag{59b}$$

As regards reservoir diameter and length sizing, no definite ways are found in the literature. Our proposed way is

$$D_{\text{res}} = (4V_{\text{res}}/\pi)^{\frac{1}{3}} \tag{60a}$$

$$L_{\text{res}} = D_{\text{res}} \tag{60b}$$

Equations (60a) and (60b) minimize the total surface area of a volume-fixed cylinder. Because the reservoir is exposed to surroundings and is connected with the secondary wick, the conductance K_{aw}, introduced in Eq. (39) to define Q', is expressed in

$$K_{aw} = 1/(1/K_{a/\text{res}} + 1/K_{\text{res}/w}) \tag{61}$$

Practical expressions for $K_{a/\text{res}}$ and $K_{\text{res}/w}$ are

$$K_{a/\text{res}} = \bar{K}_{a/\text{res}} (V_{\text{res}}/\bar{V}_{\text{res}})^{\frac{2}{3}} \tag{62a}$$

$$K_{\text{res}/w} = \bar{K}_{\text{res}/w} \left[D_{w\,\text{out}}^2 \Big/ (L_{\text{evap}} + L_{\text{res}})\right] \Big/ \left[\bar{D}_{w\,\text{out}}^2 \Big/ (\bar{L}_{\text{evap}} + \bar{L}_{\text{res}})\right] \tag{62b}$$

where the superscript macron denotes a reference value. From experimental data by Mulholland et al.,[60] the reference values become such that $\bar{K}_{a/\text{res}} = 0.10$ W/K, $\bar{K}_{\text{res}/w} = 4.63$ W/K, $\bar{V}_{\text{res}} = 200$ cm^3, and $\bar{D}_{w\,\text{out}}^2/(\bar{L}_{\text{evap}} + \bar{L}_{\text{res}}) = 0.68$ mm.

Attention is now directed to radiator panel sizing. The radiator temperature T_R is not exactly uniform but may be replaced with the fin root temperature evaluated at the condenser exit, where the radial temperature difference comes up to $\Delta T_{\text{sub}} + \Delta T_{\perp}$. Substituting Eq. (49a) for $\Delta T_{\perp}$ and taking T_v for the saturated liquid temperature, one finds

$$T_R = T_v - (1 + 1/\Phi_{\text{sub}}) \Delta T_{\text{sub}} \tag{63}$$

For a specified sink temperature T_S, the radiator surface area A_R is determined from

$$A_R = (Q + Q')/\eta_S \eta_F h_S (T_R - T_S) \tag{64}$$

where η_S is the surface effectiveness, one-sided or both-sided, η_F the fin effectiveness, and h_S the radiative heat-transfer coefficient. The fourth-power law of radiation then gives

$$h_S = \varepsilon_t \bar{\sigma} (T_R + T_S)\left(T_R^2 + T_S^2\right) \tag{65}$$

where ε_t is the surface infrared emittance and $\bar{\sigma}$ the Stefan–Boltzmann constant. A well-known formula for η_F of a rectangularly shaped fin is

$$\eta_F = \tanh \omega_F / \omega_F \tag{66}$$

where ω_F is the fin conduction parameter. A computational inversion of Eq. (66) is given in Eq. (A9), by which one can readily convert η_F into ω_F. Upon Eqs. (56) and (64), the feeder half spacing W_F is calculated from

$$W_F = A_R/2L_{\text{cond}} \tag{67}$$

An expression for ω_F is obtained from a solution of the linearized radiative–conductive fin equation. That expression is squared to become

$$k_R \delta_R = \eta_S h_S (W_F/\omega_F)^2 \tag{68}$$

where k_R is the fin thermal conductivity and δ_R the fin thickness. The product $k_R \delta_R$ then shows a required fin thermal conductance. Because engineers are interested in weight as well as dimensions, an LHP mass model is presented in Appendix C for reference.

Numerical Results and Discussion

A design code based on the above-stated analytical modeling has been developed for an LHP of basic configuration. The LHP can thus be computationally sized if Q, T_v, T_S, T_a, L_{VL}, and L_{LL} are given as design conditions. Modeling parameter values employed in this study are such that $\Phi_{\text{evap}} = 0.90$, $Bo^* = 10.0$, $\varphi_{\text{vch/VL}} = 0.833$, $q = 10.0$ kW/m^2, $(L^{(a)}/L)^*_{\text{evap}} = 1.0$, $(W/D)^*_{\text{evap}} = 4.0$, $f_H = 10.0$, $(\Delta p_{\text{wick}}/\Delta p_{\text{cap}})^* = 0.60$, $\Phi_{\text{sub}} = 0.90$, $\eta_F = 0.90$, $\varepsilon_t = 0.85$, $(\Delta p_{\text{cond}}/Q)^* = 1.0$ Pa/W, $(\Delta p_{\text{VL}}/L_{\text{VL}})^* = 40.0$ Pa/m, $(\Delta p_{\text{LL}}/L_{\text{LL}})^* = 10.0$ Pa/m, and $\Delta p_{\text{grav}}/\rho_l g = 0.10$ m. Then, unless otherwise specified, computations have been done under the condition that $T_S = 43$ K, $T_a = 313$ K, and $L_{\text{VL}} = L_{\text{LL}} = 3.0$ m. An ammonia-filled titanium-powder-wicked LHP with both-sided radiator is taken as an object of parametric design calculations because it is a popular type. Numerical results of the calculations are graphically shown in the figures to provide us with practical design curves. Every figure includes two groups of curves to compactly show the results. The bold-lined curves are drawn against the left ordinate while the fine-lined ones are drawn against the right ordinate.

Because LHPs are usually planned for a specified combination of Q and T_v, Figs. 2–7 take Q as the abscissa, ranging from 0 W to 800 W, and T_v as the curve-identifying parameter, covering an extent from 273 K to 333 K in 10 K step. Displayed in Fig. 2 are the required capillary pore radius r_c and the desired wick porosity ε_w. As expected, Fig. 2 shows that fine-pored highly porous wicks are

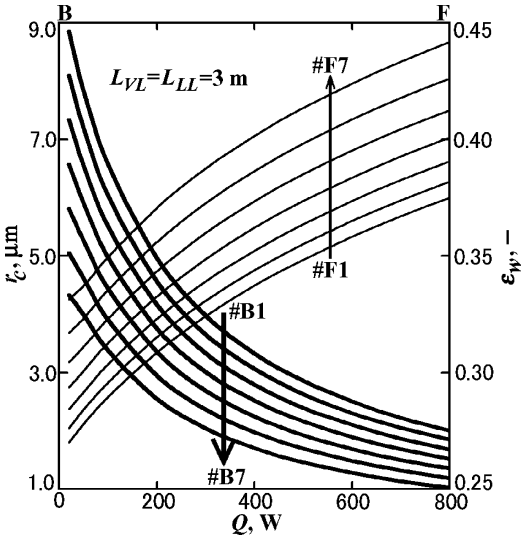

Fig. 2 Capillary pore radius and wick porosity versus heat load: #B/F1: T_v = 273 K, #B/F2: T_v = 283 K, . . . , #B/F7: T_v = 333 K in 10-K steps.

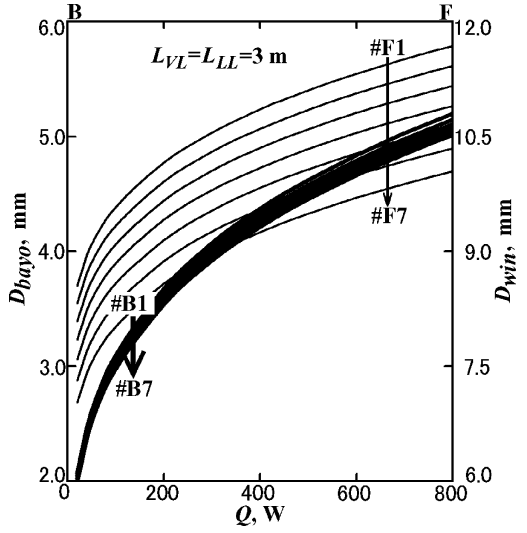

Fig. 3 Bayonet tube diameter and wick inside diameter versus heat load: #B/F1: T_v = 273 K, #B/F2: T_v = 283 K, . . . , #B/F7: T_v = 333 K in 10-K steps.

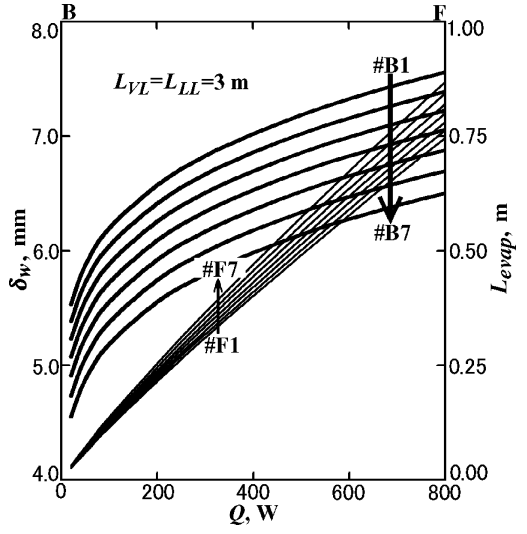

Fig. 4 Wick thickness and evaporator length versus heat load: #B/F1: T_v = 273 K, #B/F2: T_v = 283 K, . . . , #B/F7: T_v = 333 K in 10-K steps.

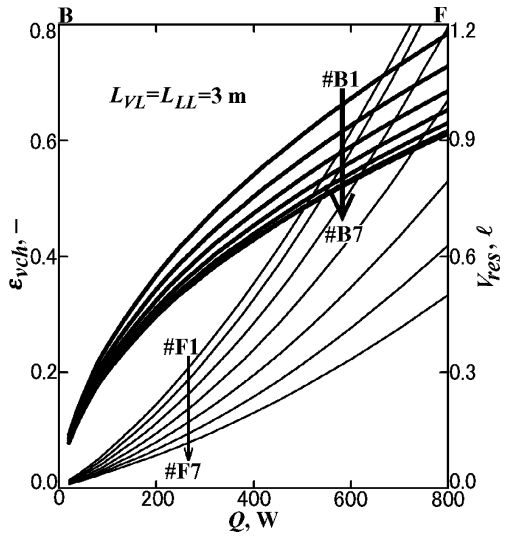

Fig. 5 Vapor-to-liquid channel cross-sectional area ratio and reservoir volume versus heat load: #B/F1: T_v = 273 K, #B/F2: T_v = 283 K, . . . , #B/F7: T_v = 333 K in 10-K steps.

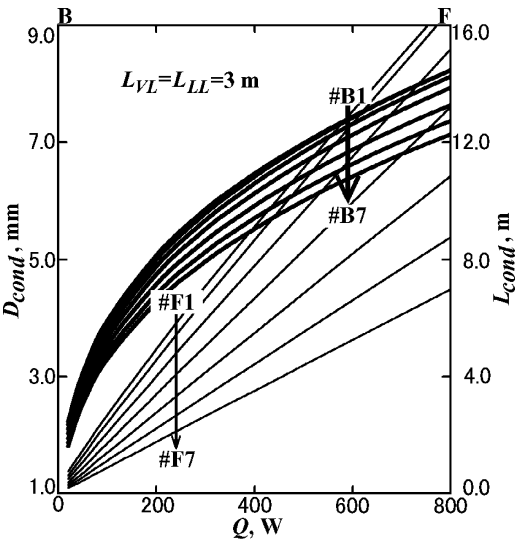

Fig. 6 Condenser tube diameter and length versus heat load: #B/F1: T_v = 273 K, #B/F2: T_v = 283 K, . . . , #B/F7: T_v = 333 K in 10-K steps.

more required as Q increases and T_v goes up. For the typical design point $Q = 300$ W and $T_v = 308$ K, one can see from curves B4/5 and F4/5 in Fig. 2 that $r_c = 2.85$ μm and $\varepsilon_w = 0.354$. Our developed wicks are such that $r_c = 1.6$ μm to 3.2 μm and $\varepsilon_w = 0.33$. Figures 3 and 4 specify radial/axial dimensions of an LHP. Displayed in Fig. 3 are the bayonet tube diameter D_{bayo} and the wick inside diameter D_{win}, whereas Fig. 4 shows the wick thickness δ_w and the evaporator length L_{evap}. It is seen from Figs. 3 and 4 that the required radial size becomes greater as Q increases and T_v decreases. Figure 4 then shows that L_{evap} almost linearly changes with Q and T_v. This results from Eqs. (19a), (20), and (21). Curves B4/5 and F4/5 in Figs. 3 and 4 indicate that $D_{\text{bayo}} = 4.0$ mm, $D_{\text{win}} = 9.7$ mm, $\delta_w = 6.3$ mm, and $L_{\text{evap}} = 0.34$ m when $Q = 300$ W and $T_v = 308$ K.

Also required in the LHP evaporator design are the vapor-to-liquid-channel cross-sectional area ratio ε_{vch} and the reservoir volume V_{res}. Figure 5 is used to find a suitable pair of these; for instance, $\varepsilon_{\text{vch}} = 0.38$ and $V_{\text{res}} = 0.22\,l$ when $Q = 300$ W and $T_v = 308$ K. Due to Eqs. (47a) and (47b), curves in Fig. 5 show the trend that ε_{vch} and V_{res} grow larger with a rise of Q and a fall of T_v. Figure 6, arranged for the LHP condencer design, gives a well-suited tube diameter D_{cond} and a required total tube length L_{cond}. Such values as $D_{\text{cond}} = 5.4$ mm and $L_{\text{cond}} = 4.6$ m are obtained from curves B4/5 and F4/5 in Fig. 6 when $Q = 300$ W and $T_v = 308$ K. A rising trend of curves in the

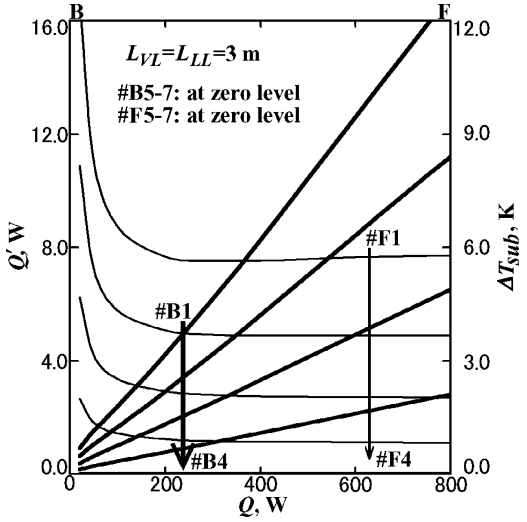

Fig. 7 Heat gain and degree of subcooling versus heat load: #B/F1: T_v = 273 K, #B/F2: T_v = 283 K, . . . , #B/F7: T_v = 333 K in 10-K steps.

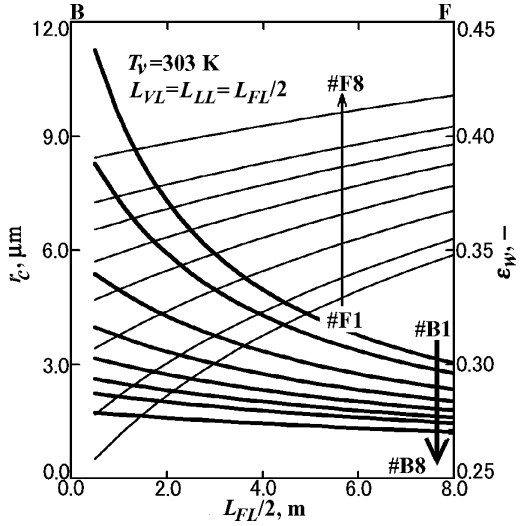

Fig. 8 Capillary pore radius and wick porosity versus vapor/liquid line length: #B/F1: Q = 50 W; #B/F2: Q = 100 W, . . . , #B/F7: Q = 600 W in 100-W steps, #B/F8: Q = 800 W.

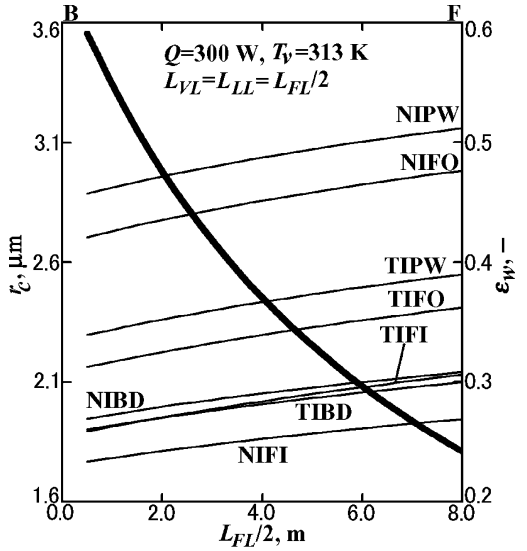

Fig. 9 Capillary pore radius and wick porosity versus vapor/liquid line length: NI/TIFI: Ni/Ti fiber, NI/TIPW: Ni/Ti powder, NI/TIBD: Ni/Ti beads, NI/TIFO: Ni/Ti foam.

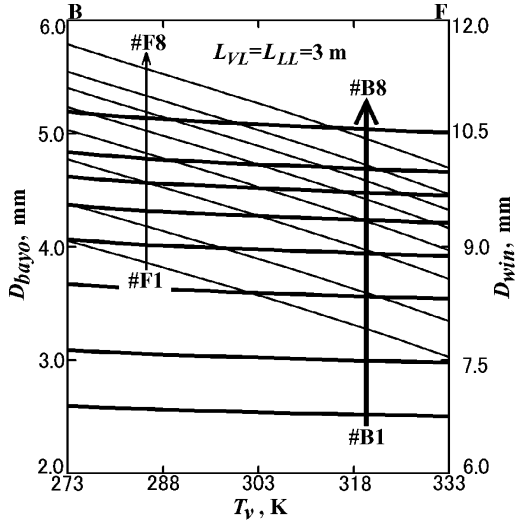

Fig. 10 Bayonet tube diameter and wick inside diameter versus vapor temperature: #B/F1: Q = 50 W; #B/F2: Q = 100 W, . . . , #B/F7: Q = 600 W in 100-W steps, #B/F8: Q = 800 W.

figure originates in Eqs. (53) and (56). Figure 7 shows the estimated heat gain Q' and the required degree of subcooling $\Delta T_{\rm sub}$. One can find Q' from curves B1–4 and $\Delta T_{\rm sub}$ from curves F1–4 when $T_v < T_a$. Because the LHP is modeled as $Q' = 0$ if $T_v \geq T_a$, curves B5–7 and F5–7 are not exposed in the figure. Any of Q' and $\Delta T_{\rm sub}$ thus depends on T_v. Those inferred from curves B1/4 and F1/4 in Fig. 7 are such that $Q' = 6.2$ W and $\Delta T_{\rm sub} = 5.6$ K when $Q = 300$ W and $T_v = 273$ K, whereas $Q' = 1.1$ W and $\Delta T_{\rm sub} = 0.88$ K when $Q = 300$ W and $T_v = 303$ K.

To specify wick characteristics, Figs. 8 and 9 display r_c and ε_w in a way different from Fig. 2. Taken as the abscissa is not Q but $L_{\rm FL}/2$, that is, the vapor/liquid line length sized as half of the total fluid line length, ranging from 0.0 m to 8.0 m. Curves in Fig. 8 are identified with the heat load Q, taking such values as 50 W, 100 W, . . . , 600 W, or 800 W. Here, the vapor temperature T_v is evenly fixed as 303 K. Curves B1/8 and F1/8 in Fig. 8 indicate that possible ranges of r_c and ε_w are from 11.3 μm and 0.26 to 3.0 μm and 0.35 when $Q = 50$ W, but from 1.7 μm and 0.39 to 1.2 μm and 0.42 when $Q = 800$ W. Figure 9 then shows the required r_c and desired ε_w values for eight kinds of wicks of interest. Considered are nickel or titanium as materials and fiber, powder, beads, or foam in structural form. All the curves in Fig. 9 are applicable to an LHP specified as $Q = 300$ W and $T_v = 313$ K. It is natural that r_c is independent of the wick type but ε_w considerably depends on it. A possible conclusion derived from curves NIPW/TIPW and NIFI/TIFI in Fig. 9 is that higher porosities are required for powdered than for fibered wicks.

There are some cases where taking T_v in place of Q as the main variable is convenient on the practical side of design. Figures 3–5 are then replaced with Figs. 10–12; where T_v is taken as the abscissa, ranging from 273 to 333 K, and Q as the curve-identifying parameter. Employed parameter values are the same as in Fig. 8. When making a rough estimate of the LHP size, one may graphically determine $D_{\rm bayo}$ and $D_{\rm win}$ from Fig. 10, δ_w and $L_{\rm evap}$ from Fig. 11, and ε_{vch} and $V_{\rm res}$ from Fig. 12. At the primary wick design, a significant sizing parameter will be $\Phi_{\rm evap}$, because δ_w and $L_{\rm evap}$ depend on $\mathcal{R}_w$ in a way defined in Eq. (19b) and Eqs. (19a),(20), and (21). Figure 13 therefore displays δ_w and $L_{\rm evap}$ as functions of $\Phi_{\rm evap}$ over a possible range from 0.78 to 0.98. Curves are then drawn under the condition that $Q = 50$ W, 100 W, . . . , or 500 W and $T_v = 313$ K. Two groups of curves in Fig. 13 show that making wicks thicker but slightly shorter is required for higher $\Phi_{\rm evap}$ values and that both δ_w and $L_{\rm evap}$ naturally increase as Q goes up. Considering the case where $Q = 300$ W in Fig. 13, one can see from curve B4 that $\delta_w = 5.5$ mm to 6.8 mm and from curve F4 that $L_{\rm evap} = 0.37$ m to 0.32 m.

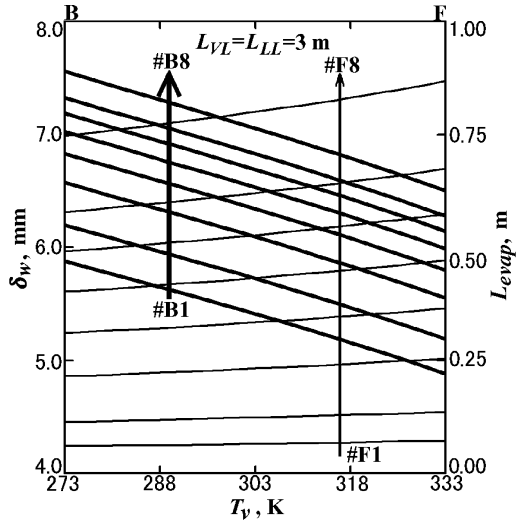

Fig. 11 Wick thickness and evaporator length versus vapor temperature: #B/F1: Q = 50 W; #B/F2: Q = 100 W, . . . , #B/F7: Q = 600 W in 100-W steps, #B/F8: Q = 800 W.

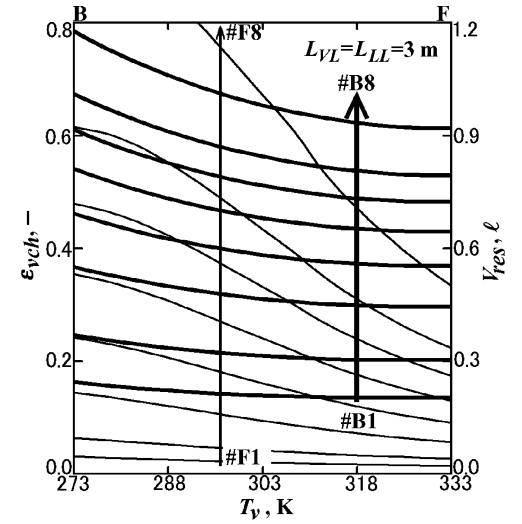

Fig. 12 Vapor-to-liquid channel cross-sectional area ratio and reservoir valume versus vapor temperature: #B/F1: Q = 50 W; #B/F2: Q = 100 W, . . . , #B/F7: Q = 600 W in 100-W steps, #B/F8: Q = 800 W.

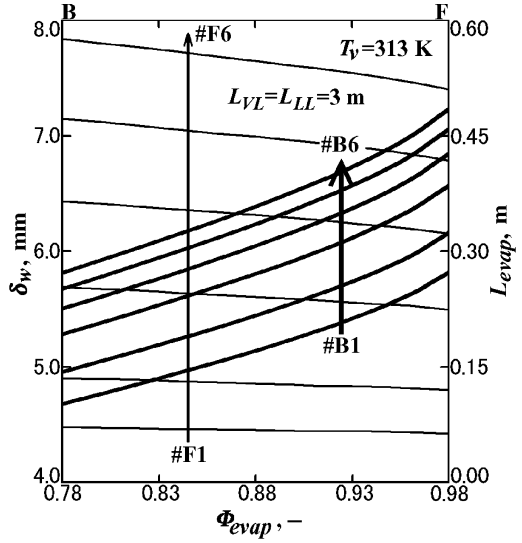

Fig. 13 Wick thickness and evaporator length versus evaporator temperature effectiveness: #B/F1: Q = 50 W; #B/F2: Q = 100 W, . . . , #B/F6: Q = 500 W in 100-W steps.

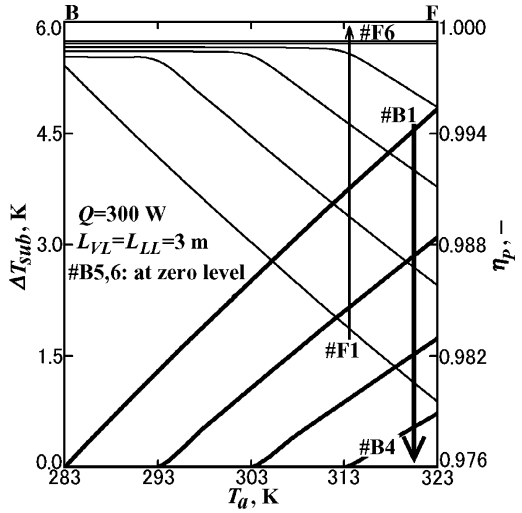

Fig. 14 Degree of subcooling and pump efficiency versus ambient temperature: #B/F1: T_v = 283 K, #B/F2: T_v = 293 K, . . . , #B/F6: T_v = 333 K in 10-K steps.

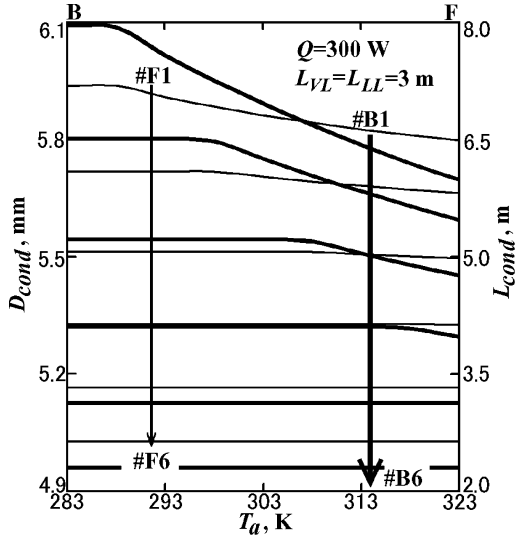

Fig. 15 Condenser tube diameter and length versus ambient temperature: #B/F1: T_v = 283 K, #B/F2: T_v = 293 K, . . . , #B/F6: T_v = 333 K in 10-K steps.

Because an LHP gains heat at the rate calculated from Eq. (39), it can be of critical importance to comprehend an effect of the ambient temperature on the LHP design. A degree of such effects, evaluated under the condition that $Q = 300$ W and $T_v = 283$ K, 293 K, . . . , or 333 K, is conceptually shown in Figs. 14 and 15; where curves are drawn against T_a extending over a range from 283 to 323 K. Displayed in Fig. 14 are the required degree of subcooling ΔT_{sub} and the resulting pump efficiency η_P. It is seen from Fig. 14 that ΔT_{sub} increases while η_P decreases as T_a goes up and as T_v goes down. Also seen from the figure is that $\Delta T_{\text{sub}} = 0.0$ K when $T_v = 323$ K or 333 K. This is due to a computational model that $Q' = 0$ if $T_v \geq T_a$. Figure 15 then displays the required condenser tube diameter D_{cond} and the required total condenser length L_{cond}. Disclosed in Fig. 15 is that both D_{cond} and L_{cond} decrease with the rise of T_a and T_v. This downward tendency results from diameter sizing such that Eqs. (42), (51), (52a), (52b), and (53) make $D_{\text{cond}}/D_{\text{LL}}$ smaller when ΔT_{sub} becomes larger. However, because of the term $Q + Q'$ in Eq. (56), an upward tendency in L_{cond} might appear in cases where the heat gain is considerably larger than our estimate.

Conclusion

This study introduced a novel concept to characterize the LHP evaporator/condenser. That concept, expressed in terms of the

temperature effectiveness, was applied to analytical modeling of an LHP of standard composition. A computationally straightforward method of the LHP design has thus been mathematically formulated to develop a design code, enabling us to specify key components of an LHP in a consistent way. That code, applicable to four kinds of wicks, has no particular restrictions in actual use. A number of curves obtained as a result of parametric design calculations are serviceable for wick/evaporator/reservoir/condenser sizing.

Appendix A: Coefficients Expressions

$$\zeta_{\text{evap}} = 2\left[1 + (\nu_v/\nu_l)(D_{\text{LL}}/D_{\text{VL}})^4\varphi_{\text{vch/VL}}^2\right] + \varepsilon_{\text{ann}}^4\Big/\left(1-\varepsilon_{\text{ann}}^2\right)\left[1+\varepsilon_{\text{ann}}^2+\left(1-\varepsilon_{\text{ann}}^2\right)\Big/\ell_n\,\varepsilon_{\text{ann}}\right] \tag{A1a}$$

$$\varepsilon_{\text{ann}} = D_{\text{bayo}}/D_{w\,\text{in}} \tag{A1b}$$

$$\zeta_{\text{port}} = \zeta_{\text{cont}}(\varphi_{\text{vch/VL}}) \tag{A2a}$$

$$\varphi_{\text{vch/VL}} = A_{\text{VL}}/A_{\text{vch}} < 1 \tag{A2b}$$

$$\varepsilon_{\text{vch}} = A_{\text{vch}}/A_{\text{lch}} = (D_{\text{VL}}/D_{w\,\text{in}})^2\Big/\varphi_{\text{vch/VL}} \tag{A2c}$$

$$\zeta_{\text{fitt}}^{(v)} = \zeta_{\text{cont}}(\varphi_{\text{VL/cond}}) \tag{A3a}$$

$$\varphi_{\text{VL/cond}} = (D_{\text{cond}}/D_{\text{VL}})^2 < 1 \tag{A3b}$$

$$\zeta_{\text{fitt}}^{(l)} = \zeta_{\text{cont}}(\varphi_{\text{cond/LL}}) \tag{A4a}$$

$$\varphi_{\text{cond/LL}} = (D_{\text{LL}}/D_{\text{cond}})^2 < 1 \tag{A4b}$$

$$\zeta_{\text{cont}} = (1-1/\varphi')^2 \tag{A5a}$$

$$\varphi' = 0.5587 + 0.5368\varphi - 1.191\varphi^2 + 1.080\varphi^3 \tag{A5b}$$

$$\alpha = 1\Big/\left\{1+[(1-\chi)/\chi](\rho_v/\rho_l)^{\frac{2}{3}}\right\} \tag{A6a}$$

$$z = 10\rho_v/\rho_l \tag{A6b}$$

$$F = 1.5[(1-\chi)/(1-\alpha)]^{0.8} \tag{A7a}$$

$$\bar{F} = \int_0^1 F\,\mathrm{d}\chi = 150\left(0.71964 - 3.6097z^{\frac{1}{3}} + 7.4174z^{\frac{2}{3}} - 6.8659z + 2.3621z^{\frac{4}{3}}\right) \tag{A7b}$$

$$\phi_v^2 = [1+75(1-\alpha)]/\alpha^{2.5} \tag{A8a}$$

$$\psi = \int_0^1 \phi_v^2\chi^{1.8}\,\mathrm{d}\chi = -0.075512 + 3.6785z^{\frac{1}{3}} - 6.8404z^{\frac{2}{3}} + 10.414z \tag{A8b}$$

$$\omega_F = 7.0734 - 18.182\eta_F + 20.177\eta_F^2 - 8.8839\eta_F^3 \tag{A9}$$

Note: Expressions of (A1a), (A6b), (A7a), and (A8a) are originally given in the literature 61–64.

Appendix B: Effective Conductivity

$$k_{\text{eff}} = k_l[1+\beta_{lw}+(1-\varepsilon_w)(1-\beta_{lw})]/[1+\beta_{lw}-(1-\varepsilon_w)(1-\beta_{lw})] \tag{B1a}$$

$$k_{\text{eff}} = k_l\beta_{lw}^{-0.34(1-\varepsilon_w)} \tag{B1b}$$

$$k_{\text{eff}} = k_w[2+\beta_{lw}-2\varepsilon_w(1-\beta_{lw})]/[2+\beta_{lw}+\varepsilon_w(1-\beta_{lw})] \tag{B2a}$$

$$k_{\text{eff}} = k_l\beta_{lw}^{-0.53(1-\varepsilon_w)} \tag{B2b}$$

$$k_{\text{eff}} = k_l[1+2\beta_{lw}+2(1-\varepsilon_w)(1-\beta_{lw})]/[1+2\beta_{lw}-(1-\varepsilon_w)(1-\beta_{lw})] \tag{B3}$$

$$k_{\text{eff}} = k_w[0.35(\varepsilon_w\beta_{lw}+1-\varepsilon_w)+0.65/(\varepsilon_w/\beta_{lw}+1-\varepsilon_w)] \tag{B4}$$

$$\beta_{\text{lw}} = k_l/k_w \tag{B5}$$

Appendix C: Mass Model

$$m_{\text{evap}} = \left[(W/D)_{\text{evap}}^{*2} - 0.785\right]\rho_{\text{evap}}D_{w\,\text{out}}^2 + 0.785\rho_w\left(D_{w\,\text{out}}^2 - D_{w\,\text{in}}^2\right) \tag{C1a}$$

$$m_{\text{cond}} = 0.524\rho_{\text{cond}}D_{\text{cond}}^2(S_{u\,\text{Al}}/S_{u\,\text{cond}}) \tag{C1b}$$

$$m_{\text{VL}} = 0.524\rho_{\text{FL}}D_{\text{VL}}^2(S_{u\,\text{Al}}/S_{u\,\text{FL}}) \tag{C1c}$$

$$m_{\text{LL}} = 0.524\rho_{\text{FL}}D_{\text{LL}}^2(S_{u\,\text{Al}}/S_{u\,\text{FL}}) \tag{C1d}$$

$$M_{\text{evap}} = m_{\text{evap}}L_{\text{evap}} \tag{C2a}$$

$$M_{\text{cond}} = m_{\text{cond}}L_{\text{cond}} \tag{C2b}$$

$$M_{\text{FL}} = m_{\text{VL}}L_{\text{VL}} + m_{\text{LL}}L_{\text{LL}} \tag{C2c}$$

$$M_{\text{res}} = 0.524\rho_{\text{res}}D_{\text{res}}^2(L_{\text{res}}+D_{\text{res}}/2)(S_{u\,\text{Al}}/S_{u\,\text{res}}) \tag{C2d}$$

$$M_{\text{rad}} = \rho_R\delta_R A_R \tag{C2e}$$

$$M_{\text{dry}} = M_{\text{evap}} + M_{\text{res}} + M_{\text{cond}} + M_{\text{rad}} + M_{\text{FL}} \tag{C3a}$$

$$M_{\text{wet}} = M_{\text{dry}} + \rho_l V_{\text{inv}} \tag{C3b}$$

References

[1] Ku, J., "Recent Advances in Capillary Pumped Loop Technology," AIAA Paper 97-3870, Aug. 1997.

[2] Maidanik, Y. F., and Fershtater, Y. G., "Theoretical Basis and Classification of Loop Heat Pipes and Capillary Pumped Loops," *10th International Heat Pipe Conference*, edited by M. Groll, Inst. for Nuclear Technology and Systems and Research Inst. for Nuclear Technology and Energy Conversion, Stuttgart, Germany, Sept. 1997, Preprint X-7.

[3] Maidanik, Y. F., "State-of-the-Art of CPL and LHP Technology," *Proceedings of the 11th International Heat Pipe Conference*, edited by S. Maezawa, The Japan Association for Heat Pipes, Tokyo, Sept. 1999, pp. 19–30.

[4] Stenger, F. J., "Experimental Feasibility Study of Water-Filled Capillary-Pumped Heat-Transfer Loops," NASA TM X-1310, Lewis Research Center, Cleveland, OH, Nov. 1966.

[5] Maidanik, Y. F., Pastukhov, V. G., Fershtater, Y. G., Smirnov-Vasiliev, K. G., Chernishev, V. F., and Dvirniy, V. V., "Development, Analytical and Experimental Investigation of Loop Heat Pipes," *7th International Heat Pipe Conference*, edited by L. Vasiliev, Luikov Heat and Mass Transfer Inst., Byelorussian Academy of Science, Minsk, BSSR, May 1990, Preprint D-21P.

[6] Nikitkin, M., and Cullimore, B., "CPL and LHP Technologies: What Are the Differences, What Are the Similarities?" SAE981587, Society of Automotive Engineers, Warrendale, PA, July 1998.

[7] Maidanik, Y. F., Fershtater, Y. G., and Solodovnik, N. N., "Loop Heat Pipes: Design, Investigation, Prospects on Use in Aerospace Technics," SAE941185, Society of Automotive Engineers, Warrendale, PA, April 1994.

[8] Wolf, D. A., Ernst, D. M., and Phillips, A. L., "Loop Heat Pipes—Their Performance and Potential," SAE941575, Society of Automotive Engineers, Warrendale, PA, June 1994.

[9] Orlov, A. A., Goncharov, K. A., Kotliarov, E. Y., Tyklina, T. A., and Ustinov, S. N., "The Loop Heat Pipe Experiment on Board the GRANAT Spacecraft," ESA-SP-400, *Proceedings of the 6th European Symposium on Space Environmental Control Systems*, Vol. 1, edited by T. D. Guyenne, ESA, Noordwijk, The Netherlands, May 1997, pp. 341–353.

[10] Goncharov, K. A., Nikitkin, M. N., Golovin, O. A., Fershtater, Y. G., Maidanik, Y. F., and Piukov, S. A., "Loop Heat Pipes in Thermal Control Systems for 'OBZOR' Spacecraft," SAE951555, Society of Automotive Engineers, Warrendale, PA, July 1995.

[11] Kozmine, D., Goncharov, K., Nikitkin, M., Maidanik, Y. F., Fershtater, Y. G., and Fiodor, S., "Loop Heat Pipes for Space Mission Mars 96," SAE961602, Society of Automotive Engineers, Warrendale, PA, July 1996.

[12] Baker, C. L., Bienert, W. B., and Ducao, A. S., "Loop Heat Pipe Flight Experiment," SAE981580, Society of Automotive Engineers, Warrendale, PA, July 1998.

[13] Lashley, C., Krein, S., and Barcomb, P., "Deployable Radiators—A Multi-discipline Approach," SAE981691, Society of Automotive Engineers, Warrendale, PA, July 1998.

[14] Douglas, D., Ku, J., and Kaya, T., "Testing of the Geoscience Laser Altimeter System (GLAS) Prototype Loop Heat Pipe," AIAA Paper 99-0473, Jan. 1999.

[15]Mena, F., Supper, W., and Puillet, C., "Design and Development of Loop Heat Pipes," 2000-01-2315, Society of Automotive Engineers, Warrendale, PA, July 2000.

[16]Schlitt, R., Dubois, M., Ounougha, L., and Supper, W., "COM2PLEX—A Combined European LHP Experiment on SPACEHAB/QUEST," 2000-01-2457, Society of Automotive Engineers, Warrendale, PA, July 2000.

[17]Pastukhov, V. G., Maidanik, Y. F., and Chernyshova, M. A., "Development and Investigation of Miniature Loop Heat Pipes," 1999-01-1983, Society of Automotive Engineers, Warrendale, PA, July 1999.

[18]Yun, S. J., Wolf, D., and Kroliczek, E., "Design and Test Results of Reversible Loop Heat Pipe," 1999-01-2053, Society of Automotive Engineers, Warrendale, PA, July 1999.

[19]Yun, S. J., Wolf, D., and Kroliczek, E., "Design and Test Results of Multi-Evaporator Loop Heat Pipes," 1999-01-2051, Society of Automotive Engineers, Warrendale, PA, July 1999.

[20]Goncharov, K., Golovin, O., and Kolesnikov, V., "Loop Heat Pipe with Several Evaporators," 2000-01-2407, Society of Automotive Engineers, Warrendale, PA, July 2000.

[21]Ku, J., "Operating Characteristics of Loop Heat Pipes," 1999-01-2007, Society of Automotive Engineers, Warrendale, PA, July 1999.

[22]Wolf, D. A., and Bienert, W.B., "Investigation of Temperature Control Characteristics of Loop Heat Pipes," SAE941576, Society of Automotive Engineers, Warrendale, PA, June 1994.

[23]Sasin, V. Y., Zelenov, I. A., Zuev, V. G., and Kotlyarov, E. Y., "Mathematical Model of a Capillary Loop Heat Pipe with a Condenser-Radiator," SAE901276, Society of Automotive Engineers, Warrendale, PA, July 1990.

[24]Goncharov, K. A., Kotlyarov, E. Y., Smirnov, F. Y., Schlitt, R., Beckmann, K., Meyer, R., and Müller, R., "Investigation of Temperature Fluctuations in Loop Heat Pipes," SAE941577, Society of Automotive Engineers, Warrendale, PA, June 1994.

[25]Maidanik, Y., Solodovnik, N., and Fershtater, Y., "Investigation of Dynamic and Stationary Characteristics of a Loop Heat Pipe," LA-UR-97-1500, *Proceedings of the 9th International Heat Pipe Conference*, Vol. 2, edited by M. A. Merrigan, Los Alamos National Laboratory and Univ. of New Mexico, Los Alamos, NM, May 1995, pp. 1002–1006.

[26]Cheung, K., Hoang, T. T., Ku, J., and Kaya, T., "Thermal Performance and Operational Characteristics of Loop Heat Pipe (NRL LHP)," SAE981813, Society of Automotive Engineers, Warrendale, PA, July 1998.

[27]Kaya, T., and Ku, J., "A Parametric Study of Performance Characteristics of Loop Heat Pipes," 1999-01-2006, Society of Automotive Engineers, Warrendale, PA, July 1999.

[28]Baumann, J., Cullimore, B., Yendler, B., and Buchan, E., "Noncondensible Gas, Mass, and Adverse Tilt Effects on the Start-up of Loop Heat Pipes," 1999-01-2048, Society of Automotive Engineers, Warrendale, PA, July 1999.

[29]Baumann, J., Cullimore, B., Ambrose, J., Buchan, E., and Yendler, B., "A Methodology for Enveloping Reliable Start-up of LHPs," AIAA Paper 2000-2285, June 2000.

[30]Gluck, D., Gerhart, C., and Stanley, S., "Startup of a Loop Heat Pipe with Initially Cold Evaporator, Compensation Chamber and Condenser," *Proceedings of the 11th International Heat Pipe Conference*, edited by S. Maezawa, The Japan Association for Heat Pipes, Tokyo, Sept. 1999, pp. 311–316.

[31]Ku, J., Ottenstein, L., Rogers, P., and Cheung, K., "Investigation of Low Power Operation in a Loop Heat Pipe," 2001-01-2192, Society of Automotive Engineers, Warrendale, PA, July 2001.

[32]Ku, J., Ottenstein, L., Rogers, P., and Cheung, K., "Capillary Limit in a Loop Heat Pipe with a Single Evaporator," 2002-01-2502, Society of Automotive Engineers, Warrendale, PA, July 2002.

[33]Bienert, W. B., and Wolf, D. A., "Temperature Control with Loop Heat Pipes: Analytical Model and Test Results," LA-UR-97-1500, *Proceedings of the 9th International Heat Pipe Conference*, Vol. 2, edited by M. A. Merrigan, Los Alamos National Laboratory and Univ. of New Mexico, Los Alamos, NM, May 1995, pp. 981–988.

[34]Kaya, T., Hoang, T. T., Ku, J., and Cheung, M. K., "Mathematical Modeling of Loop Heat Pipes," AIAA Paper 99-0477, Jan. 1999.

[35]Kaya, T., Hoang, T. T., "Mathematical Modeling of Loop Heat Pipes and Experimental Validation," *Journal of Thermophysics and Heat Transfer*, Vol. 13, No. 3, 1999, pp. 314–320.

[36]Hoang, T. T., and Kaya, T., "Mathematical Modeling of Loop Heat Pipes with Two-Phase Pressure Drop," AIAA Paper 99-3448, June–July 1999.

[37]Wrenn, K. R., Krein, S. J., Hoang, T. T., and Allen, R. D., "Verification of a Transient Loop Heat Pipe Model," 1999-01-2010, Society of Automotive Engineers, Warrendale, PA, July 1999.

[38]Cullimore, B., and Baumann, J., "Steady-State and Transient Loop Heat Pipe Modeling," 2000-01-2316, Society of Automotive Engineers, Warrendale, PA, July 2000.

[39]Pauken, M., and Rodriguez, J. I., "Performance Characterization and Model Verification of a Loop Heat Pipe," 2000-01-2317, Society of Automotive Engineers, Warrendale, PA, July 2000.

[40]Hoff, C. J., and Rogers, P. D., "Correlation of a SINDA/FLUINT Model for a Switchbox Loop Heat Pipe," NHTC2000-12160, American Society of Mechanical Engineers, New York, Aug. 2000.

[41]Maidanik, Y. F., Fershtater, Y. G., and Solodovnik, N. N., "Design and Investigation of Methods of Regulation of Loop Heat Pipes for Terrestrial and Space Applications," SAE941407, Society of Automotive Engineers, Warrendale, PA, June 1994.

[42]Borodkin, A. A., Sasin, V. Y., Kotliarov, E. Y., and Goncharov, K. A., "Loop Heat Pipes Heat Transfer Characteristics Analysis by Using Nomograms," SAE961566, Society of Automotive Engineers, Warrendale, PA, July 1996.

[43]Furukawa, M., "Off-Design State Predictions of a Commonly Configured Loop Heat Pipe," *Transactions of the Japan Society for Aeronautical and Space Sciences*, Vol. 46, No. 151, 2003, pp. 36–41.

[44]Parker, M. L., Drolen, B. L., and Ayyaswamy, P. S., "Loop Heat Pipe Performance—Is Subcooling Required?" AJTE99-6285, American Society of Mechanical Engineers, New York, March 1999.

[45]Hoang, T. T., and Ku, J., "Heat and Mass Transfer in Loop Heat Pipes," HT2003-47366, American Society of Mechanical Engineers, New York, July 2003.

[46]Kaya, T., and Ku, J., "Thermal Operational Characteristics of a Small-Loop Heat Pipe," *Journal of Thermophysics and Heat Transfer*, Vol. 17, No. 4, 2003, pp. 464–470.

[47]Williams, J. L., Keshock, E. G., and Wiggins, C. L., "Development of a Direct Condensing Radiator for Use in a Spacecraft Vapor Compression Refrigeration System," *Journal of Engineering for Industry*, Vol. 95, No. 4, 1973, pp. 1053–1064.

[48]Weisman, J., Duncan, D., Gibson, J., and Crawford, T., "Effect of Fluid Properties and Pipe Diameter on Two-Phase Flow Patterns in Horizontal Lines," *International Journal of Multiphase Flow*, Vol. 5, No. 6, 1979, pp. 437–462.

[49]Chi, S. W., "Capillary Limitation and Temperature Characteristics," *Heat Pipe Theory and Practice: A Source Book*, Hemisphere, Washington, DC, 1976, pp. 33–78.

[50]Faghri, A., "Steady Hydrodynamic and Thermal Characteristics," *Heat Pipe Science and Technology*, Taylor and Francis, New York, NY, 1995, pp. 115–220.

[51]Ambrose, J. H., Chow, L. C., and Beam, J. E., "Capillary Flow Properties of Mesh Wicks," *Journal of Thermophysics and Heat Transfer*, Vol. 4, No. 3, 1990, pp. 318–324.

[52]Hanlon, M. A., and Ma, H. B., "Evaporation Heat Transfer in Sintered Porous Media," *Journal of Heat Transfer*, Vol. 125, No. 4, 2003, pp. 644–652.

[53]Alazmi, B., and Vafai, K., "Analysis of Variants within the Porous Media Transport Models," *Journal of Heat Transfer*, Vol. 122, No. 2, 2000, pp. 303–326.

[54]Tan, K. K., Sam, T., and Jamaludin, H., "The Onset of Transient Convection in Bottom Heated Porous Media," *International Journal of Heat and Mass Transfer*, Vol. 46, No. 15, 2003, pp. 2857–2873.

[55]Yip, F. C., "Design Parameter for Assessing Wicking Capabilities of Heat Pipes," *Journal of Spacecraft and Rockets*, Vol. 13, No. 4, 1976, pp. 237–243.

[56]Dunn, P., and Reay, D. A., "Practical Design Considerations," *Heat Pipes*, 3rd ed., Pergamon, Oxford, England, UK, 1982, pp. 90–137.

[57]Peterson, G. P., and Fletcher, L. S., "Effective Thermal Conductivity of Sintered Heat Pipe Wicks," *Journal of Thermophysics and Heat Transfer*, Vol. 1, No. 4, 1987, pp. 343–347.

[58]Bhattacharya, A., Calmidi, V. V., and Mahajan, R. L., "Thermophysical Properties of High Porosity Metal Foams," *International Journal of Heat and Mass Transfer*, Vol. 45, No. 5, 2002, pp. 1017–1031.

[59]Mishkinis, D., Ochterbeck, J. M., Sodtke, C., Ku, J., and Butler, D., "Non-dimensional Analysis and Scaling Issues in Loop Heat Pipes," AIAA Paper 2003-0341, Jan. 2003.

[60]Mulholland, G., Gerhart, C., Gluck, D., and Stanley, S., "Comparison Between Analytical Predictions and Experimental Data for a Loop Heat Pipe," *Space Technology and Applications International Forum—1999*, AIP Conference Proceedings 458, edited by M. S. El-Genk, American Inst. of Physics, Springer-Verlag, New York, Jan.–Feb. 1999, pp. 805–810.

[61]Knudsen, J. G., and Katz, D. L., "Heat Transfer and Pressure Drop in Annuli—Measurements on Plain and Transverse Fin Tubes Using Water," *Chemical Engineering Progress*, Vol. 46, No. 10, 1950, pp. 490–500.

[62]Zivi, S. M., "Estimation of Steady-State Steam Void-Fraction by Means of the Principle of Minimum Entropy Production," *Journal of Heat Transfer*, Vol. 86, No. 2, 1964, pp. 247–252.

[63]Davis, E. J., and David, M. M., "Heat Transfer to High-Quality Steam–Water Mixtures Flowing in a Horizontal Rectangular Duct," *The Canadian Journal of Chemical Engineering*, Vol. 39, No. 3, 1961, pp. 99–105.

[64]Wallis, G. B., "Annular Flow," *One-Dimensional Two-Phase Flow*, McGraw–Hill, New York, 1969, pp. 315–374.